Title
Dynamic Simulation of a Pressurized 220kW Solid Oxide Fuel-Cell–Gas-Turbine Hybrid System: Modeled Performance Compared to Measured Results

Journal
Journal of Electrochemical Energy Conversion and Storage, 3(1)

ISSN
1550-624X

Authors
Roberts, RA
Brouwer, J

Publication Date
2006-02-01

DOI
10.1115/1.2133802

Dynamic Simulation of a Pressurized 220 kW Solid Oxide Fuel-Cell–Gas-Turbine Hybrid System: Modeled Performance Compared to Measured Results

R. A. Roberts

J. Brouwer
e-mail: jb@nfcrc.uci.edu

National Fuel Cell Research Center,
University California,
Irvine, Irvine, CA 92697-3550

Hybrid fuel-cell–gas-turbine (FC/GT) systems are technologically advanced systems that are promising for electric power generation with ultralow emissions and high efficiency for a large range of power plant sizes. A good understanding of the steady-state and dynamic performance of a FC/GT system is needed in order to develop and advance this hybrid technology. In this work, a detailed dynamic model of a solid oxide fuel cell/gas turbine (SOFC/GT) system has been developed. The system that is simulated represents the 220 kW *SOFC/GT hybrid system developed by Siemens Westinghouse. Results of the dynamic model and experimental data gathered during the operation and testing of the* 220 kW *SOFC/GT at the National Fuel Cell Research Center are compared and presented.* [DOI: 10.1115/1.2133802]

Introduction and Background

Fuel cell/gas turbine (FC/GT) hybrids integrate high-temperature fuel cells with gas turbine engines in a manner that converts fuel cell thermal energy through turbo machinery to power compressors and/or electric generators. In both thermodynamic simulation and experiment, these hybrid systems have demonstrated lower environmental impact compared to conventional combustion-driven power plants. Lower carbon dioxide emissions can be achieved through higher fuel-to-electrical efficiencies, while NO_x and other criteria pollutant emissions are greatly reduced by primary electrochemical conversion of the fuel versus the combustion process of conventional plants [1]. In this work, a dynamic model of a hybrid system is developed and applied to analyze a specific hybrid cycle that is applicable to distributed generation. More complex cycles have been considered for larger scale power plants that may utilize a combined cycle to drive the efficiency up and the environmental impact down [2].

Today much work is being done to reduce the cost and increase the reliability of solid oxide fuel cell (SOFC) systems. Several cell geometries are being advanced by fuel cell manufacturers including tubular and planer SOFC designs, and even cell geometries that combine planer and tubular features. Each geometry has its advantages and disadvantages with regard to thermal expansion compliance, power density, potential cost, manufacturability, and internal resistivity [3]. Many companies are advancing these different types of SOFCs, but no commercial products exist today. Only demonstration and prototype systems have been built and tested to date.

Mathematical models provide a cost-effective and efficient tool in aiding the development of SOFCs and SOFC/GT systems. Several entities around the world have developed steady-state simulation capabilities for FC/GT systems. These research groups include efforts at the Georgia Institute of Technology, University of Genova, NFCRC, Nanyang Technical University, and others [2–8]. Dynamic FC/GT simulation capabilities are less common, but increasingly being developed as the demand for dynamic understanding and controls development grows. Examples of previous dynamic simulation efforts include work at the National Energy Technology Laboratory and FuelCell Energy among others [9–13]. Model validation is very important, and there remains a great need to produce experimental hybrid system data.

To date there have been two hybrid systems built and successfully demonstrated. The first uses an atmospheric fuel cell located after the turbine exhaust has been built and demonstrated by FuelCell Energy that integrated a molten carbonate fuel cell and a Capstone C30 gas turbine. This system successfully ran for 2900 h in grid-connected mode at 51.7% fuel-to-electrical efficiency. See Ghezel-Ayagh et al. [14] for more information on this system. The second system uses a pressurized fuel cell located between the compressor and turbine, which is the system of direct interest to the current work.

Experiment Description

Siemens Westinghouse developed the very first pressurized SOFC/GT hybrid system using their tubular SOFC stack design. This system, presented in Fig. 1, was tested at the NFCRC with support from Southern California Edison, the U.S. Department of Energy, and others. The system was designed, constructed, and tested to demonstrate and prove the hybrid concept. The system operated for over 2900 h and produced up to 220 kW at fuel-to-electricity conversion efficiencies of up to 53%. In parallel, NFCRC developed dynamic simulation capabilities for each of the system components together with a simulation framework for modeling and developing control strategies for integrated SOFC/GT systems.

A diagram of the integrated SOFC/GT system is presented in Fig. 2. This system is comprised of a tubular SOFC with integrated internal reformer and anode off-gas oxidizer as illustrated in Fig. 3. These components (stack, reformer) are placed between the compressor and turbine so that they operate under pressurized conditions. The gas turbine is a dual shaft Ingersoll-Rand 75 kW

Manuscript received February 8, 2005; final manuscript received August 19, 2005. Review conducted by Subhash C. Singhal.

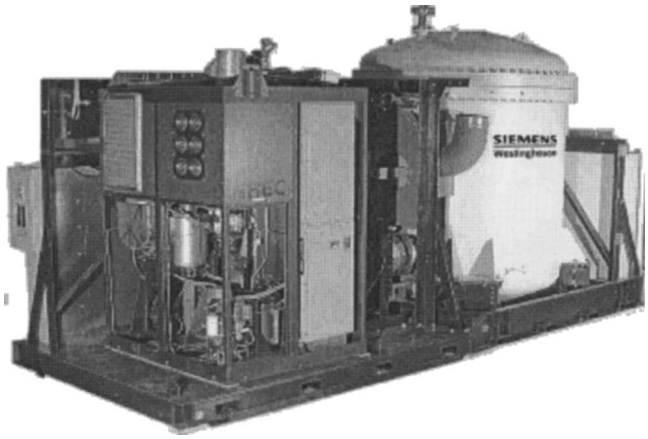

Fig. 1 Pressurized 220 kW SOFC/gas turbine hybrid

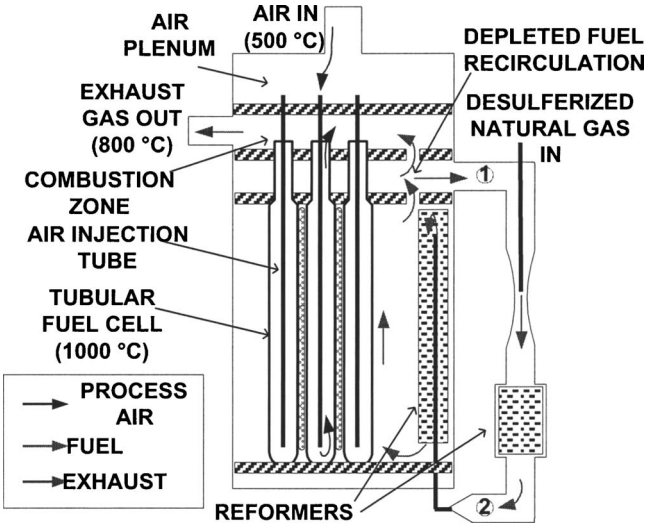

Fig. 3 Tubular SOFC stack design

gas turbine. The integrated cycle also includes a recuperative heat exchanger and a separate turbine generator set (see Fig. 2). Note that there are also two bypass valves that can divert flow around the heat exchanger and around the SOFC.

Dynamic and steady-state data were gathered during operation. Nominally, the SOFC produced 180 kWe, whereas the GT produced 40 kWe of the total power. The dynamic data produced by the SOFC/GT system was primarily gathered during start-up and shutdown. The primary goal of the experimental effort was to demonstrate the hybrid concept for 3000 h of steady-state operation without detailed investigation of dynamic responses to perturbations.

Under nominal operating conditions, the SOFC stack was pressurized to three atmospheres, resulting in improved efficiency and increased power density through reduction in polarization losses and increased Nernst potential. The SOFC stack produces 100 kWe at atmospheric pressure, whereas in the hybrid configuration it produced as much as 180 kWe. A more detailed description of the system is presented in other works [7,15].

Model Description

The equations that govern the dynamic performance of each of the system components are solved in a modular fashion for each of the components of the 220 kW hybrid system in a MATLAB/SIMULINK™ format. The models were designed and constructed to be reliable and robust. All of the models are based on the fundamental mass, momentum, and energy conservation equations plus

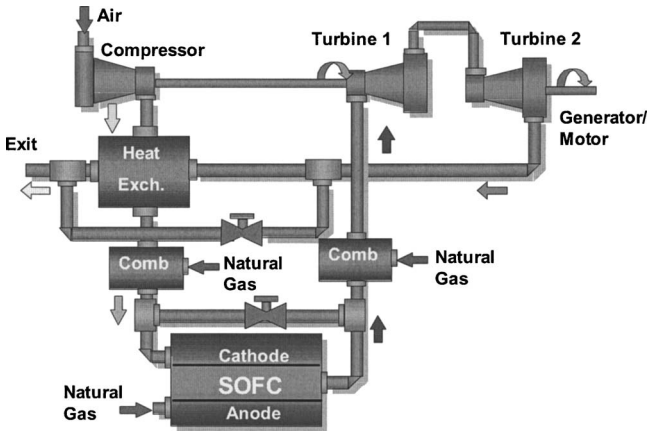

Fig. 2 Diagram of the pressurized 220 kW SOFC/gas turbine hybrid system

detailed solutions of electrochemical, chemical, and heat transfer processes.

SOFC Model. The SOFC model developed for the current application is a simplified bulk model that simulates the overall performance of a pressurized tubular SOFC. The current model does not capture the spatial variations of operating parameters throughout the SOFC stack. This simplified model is deemed sufficient for simulating a complete hybrid system. However, spatially resolved models may be required to more accurately simulate the performance of specific SOFC stack designs and to garner more insights into stack behavior. Such models have been developed previously at the NFCRC and will be considered for future integration in a full hybrid system model [16,17].

The governing equations of the SOFC model are introduced, starting with the Nernst potential Eq. (1), which provides the reversible cell potential for a given fuel and oxidant composition,

$$E = E_0 + \frac{R_u T}{2F} \ln\left(\frac{\mathbf{X}_{H_2} \mathbf{X}_{O_2}^{1/2}}{\mathbf{X}_{H_2O}} P_{\text{cathode}}^{1/2} \right) \tag{1}$$

Although Eq. (1) solves for ideal cell potential, the actual cell potential for any fuel cell under real operating conditions will be reduced due to irreversibilities referred to as polarizations or overpotential losses.

The modeling of realized cell voltage can be achieved by calculating each of the three primary overpotentials (activation, ohmic, and concentration) in bulk fashion and subtracting them from the ideal Nernst potential as in

$$V_{\text{cell}} = E - \eta_A - \eta_C - \eta_R \tag{2}$$

where V_{cell} is the actual cell voltage for a given current, η_A is the activation polarization loss, η_C is the concentration polarization loss, and η_R is the ohmic polarization loss. Calculation of these polarizations is based on a first-principles understanding of the overall performance of a fuel cell. For a given temperature and pressure, all three polarizations are typically only a function of current demand.

The loss associated with sluggish kinetics that is attributed to low temperatures, lack of availability of active catalytic cell sites, triple-phase boundary kinetics, and/or concentration of reactants at the reacting site is modeled using a relationship for activation polarization. This polarization is more dominant at low current densities, but at higher current densities the Tafel equation is used. The Tafel activation polarization equation is

Table 1 SOFC electrochemistry parameters

SOFC Parameter	Value	Unit
i_o	400	A/m^2
i_L	4000	A/m^2
R_{eff}	1.7E-05	ohm-m^2
α	0.6	

$$\eta_A = \frac{R_u T}{\alpha n F} \ln\left(\frac{i}{i_0}\right) \tag{3}$$

The key parameter that determines activation polarization for a specific fuel cell is i_o, which is the exchange current density. Exchange current density is associated with the catalytic activity of a particular cell and corresponds to the rate at which the electrodes exchange ions with the electrolyte under equilibrium conditions (no net current flow). For Eq. (3) to be valid $i > i_o$. α represents the distribution of intermediate species at the triple phase boundary, indicating whether these species more closely resemble reactants or products. α has a value between zero and one (usually taken to be 0.5). The values for i_o and α are given in Table 1.

The irreversibility associated with diffusion limits and concentration gradients near the active cell surface is modeled by

$$\eta_C = -\frac{R_u T}{nF} \ln\left(1 - \frac{i}{i_L}\right) \tag{4}$$

The new term here is i_L, which is the limiting current density. Limiting current density corresponds to the maximum current that the fuel cell can produce to equal the maximum supply speed of reactants. To avoid this polarization, the fuel cell is usually operated at lower current densities or at higher pressures (if power density is a concern). The value for i_L is given in Table 1.

Since activation polarization is reduced at high temperature and high-temperature fuel cells are typically operated at relatively low current density, ohmic polarization is usually the most significant electrochemical loss. At normal operating conditions, this ohmic loss is primarily due to low ionic conductivity of the electrolyte and/or low electrical conductivity of associated interconnect materials. Resistance can also be high if the cell is operating at a temperature below the optimum due to the strong temperature dependence of electrolyte ionic resistivity. The potential loss associated with cell resistance is

$$\eta_R = iR_{\text{eff}} \tag{5}$$

where i is the current density and R_{eff} is the effective overall cell resistance. Several fuel cell parameters affect the cell resistance, including inherent electrolyte ionic conductivity, electrolyte thickness, electrode and interconnect electronic conductivities, and geometry of the electrolyte affects the internal resistance. Thinner electrolyte layers can be designed to reduce ionic ohmic polarization, but the thickness is bound by the requirements of the cell to endure structural stresses produced by different thermal expansion of the materials that are sandwiched together. The value for R_{eff} is given in Table 1.

The SOFC model incorporates the dynamic equations that solve for conservation of mass or species, momentum, and energy. For species conservation the equation assuming a well-stirred reactor approach is used

$$V_{cv} C \frac{d\mathbf{X}}{dt} = \dot{N}_{\text{in}}(\mathbf{X}_{\text{in}} - \mathbf{X}) - \mathbf{X}\sum \mathbf{R} + \mathbf{R} \tag{6}$$

There are seven species considered: methane, carbon monoxide, carbon dioxide, hydrogen, water, nitrogen, and oxygen. Using Faraday's law of electrolysis Eq. (7), the electrochemistry vectors for the reaction rates in the SOFC anode and cathode become equations Eqs. (8) and (9) for the anode and cathode, respectively,

$$r_j = \frac{ai}{nF} \tag{7}$$

$$\mathbf{R}_{\mathbf{anode,e}} = A_{\text{cell}}\left[0\ 0\ 0\ -\frac{i}{2F}\ +\frac{i}{2F}\ 0\ 0\right] \tag{8}$$

$$\mathbf{R}_{\mathbf{cathode,e}} = A_{\text{cell}}\left[0\ 0\ 0\ 0\ 0\ 0\ -\frac{i}{4F}\right] \tag{9}$$

Reformation and water-gas-shift chemical reactions occur simultaneously with the electrochemical reactions in the anode compartment of the SOFC. The reaction vector for the internal reformation chemical reactions is added to the electrochemistry reaction vector and inserted into Eq. (6) to solve for dynamic species conservation.

The internal reformation model considers the chemical kinetics of three concurrent chemical reactions, steam reformation of methane, and water-gas shift as follows:

$$CH_4 + H_2O \rightarrow CO + 3H_2 \tag{10}$$

$$CO + H_2O \rightarrow CO_2 + H_2 \tag{11}$$

$$CH_4 + 2H_2O \rightarrow CO_2 + 4H_2 \tag{12}$$

The forward rates of these steam reformation and water-gas shifts are determined by Arrhenius rate expressions. The reformation model uses rates that are consistent with the use of typical nickel-based catalysts [18]. This should be reasonable considering the nickel-YSZ composition of the cathode and nickel felt electrical connection materials in the anode compartment. The rate equation of reaction Eq. (10) is

$$R_1 = k_1\left(\frac{P_{CH_4}P_{H_2O}}{P_{H_2}^{2.5}} - \frac{P_{CO}P_{H_2}^{0.5}}{K_{p1}}\right) \Big/ DEN^2 \tag{13}$$

The rate of reaction Eq. (11) is

$$R_2 = k_2\left(\frac{P_{CO}P_{H_2O}}{P_{H_2}} - \frac{P_{CO_2}}{K_{p2}}\right) \Big/ DEN^2 \tag{14}$$

The rate of reaction Eq. (12) is

$$R_3 = k_3\left(\frac{P_{CH_4}P_{H_2O}^2}{P_{H_2}^{3.5}} - \frac{P_{CO_2}P_{H_2}^{0.5}}{K_{p3}}\right) \Big/ DEN^2 \tag{15}$$

The denominator used in each of the reaction rate expressions above is

$$DEN = 1 + K_{CO}P_{CO} + K_{H_2}P_{H_2} + K_{CH_4}P_{CH_4} + \frac{K_{H_2O}P_{H_2O}}{P_{H_2}} \tag{16}$$

According to the Arrhenius equation and van't Hoff equation, the reaction constants k_i (i=1–3) and K_j (j=CO, CH_4, H_2O, or H_2) in the above equations can be calculated from the preexponential factors A_i and A_j, and the absorption parameters E_i and ΔH_j from the following equations:

$$k_i = A_i \exp\left(-\frac{E_i}{RT}\right) \tag{17}$$

$$K_j = A_j \exp\left(-\frac{\Delta H_j}{RT}\right) \tag{18}$$

The constants used in the current model are presented in Tables 2 and 3. CO is assumed to be consumed/created only by water-gas shift and steam reformation. Direct electrochemical oxidation of CO and hydrocarbons is possible under current anodic conditions, but it occurs at a sufficiently slow rate that this assumption has

Table 2 Reformation constants

Rate Constant	Activation energy (kJ/mol)	Pre-exponential factor	Rate Constant	Heat of adsorption (kJ/mol)	Pre-exponential factor
k_1	240.1	1.336×10^{15} (kmol·MPa$^{(0.5)}$/kg$_{cat}$·h)	K_{CO}	-70.65	8.23×10^{-4} (MPa^{-1})
k_2	67.13	1.955×10^{7} (kmol/kg$_{cat}$·h·MPa)	K_{CH4}	-38.28	6.65×10^{-3} (MPa^{-1})
k_3	243.9	3.22×10^{14} (kmol·MPa$^{(0.5)}$/kg$_{cat}$·h)	K_{H2O}	88.68	1.77×10^{5} (unitless)
			K_{H2}	-82.9	6.12×10^{-8} (MPa^{-1})

been shown to be reasonable in previous studies [19].

The SOFC model solves for the energy balance between the anode and cathode gas streams and the fuel cell materials. The energy balance for the cell materials (electrode-electrolyte assembly) is solved using Eq. (19). There is heat generated within the porous fuel cell electrode-electrolyte assembly where the hydrogen is being electrochemically oxidized. Based on the lower heating value of hydrogen, the energy that is not being converted to electrical energy produces heat in the SOFC stack as in Eq. (20)

$$\frac{d\rho C_{\text{mass}} T V_{cv}}{dt} = \dot{E}_{\text{in}} - \dot{E}_{\text{out}} + Q_{\text{gen}} \tag{19}$$

$$Q_{\text{gen}} = \left(\frac{\Delta H_{f,\text{H}_2\text{O}(g)}}{nF} - V_{\text{cell}} \right) i \tag{20}$$

As for the anode and cathode gases, Eq. (21) solves the energy balance for each of these control volumes

$$\frac{dCC_{v,\text{molar}} T V_{cv}}{dt} = \dot{E}_{\text{in}} - \dot{E}_{\text{out}} \tag{21}$$

The gas stream flows are assumed to be fully developed laminar flow. This assumption permits the use of an altered form of the Darcy equation Eq. (22) for the solution of momentum conservation (calculating the fuel cell pressure drop) as follows:

$$\Delta P = f \frac{L}{D_h} \frac{\rho v^2}{2} \tag{22}$$

where ΔP is the pressure drop, f is the friction factor, L is the characteristic length, ρ is density, v is average velocity, and D_h is the hydraulic diameter.

The tubular SOFC stack is encased by a stainless-steel casing. There are some leaks within the casing inherent to the seal-less design of Siemens Westinghouse's SOFC stacks. Therefore, a small fraction of the fuel bypasses the tubular cells and directly oxidizes within the combustion chamber or pressure chamber. In this study, it was assumed that 3% of the fuel bypasses the cells and is directly oxidized through combustion.

Table 3 Equilibrium constants

Equilibrium constant		Dimensions
K_{p1}	= $1.198 \times 10^{11} * \exp(-26830/T)$	$(\text{MPa})^2$
K_{p2}	= $1.77 \times 10^{-2} * \exp(4400/T)$	$(\text{MPa})^0$
K_{p3}	= $K_{p1} * K_{p2}$	$(\text{MPa})^2$

Heat Exchanger and Combustor Model. The recuperator heat exchanger, SOFC heat exchanger, and combustor models are one-dimensional in the streamwise direction. The heat exchangers solve the conservation equations for mass, momentum, and energy. The same equations (Eqs. (19)–(22)) are used for the heat exchangers and combustor models except that there is no heat generation in the heat exchanger models.

Gas Turbine Model. A transient mathematical model of a gas turbine system has been developed using the same MATLAB/SIMULINK framework. The model predicts the behavior of a lumped parameter compressor and expander attached via rotating shaft. The dynamic expressions that account for gas compressibility and mass storage are solved in separate diffuser volumes as depicted in Fig. 4. A generator load can be applied to the shaft, or the system can operate as a turbocharger.

The current one-dimensional lumped parameter approach is flexible to allow the incorporation of semi-empirical data from a specific production or prototype gas turbine. The semi-empirical data that is used in the current dynamic gas turbine modeling approach is in the form of nondimensionalized compressor and turbine "maps." These compressor and turbine maps provide steady-state mass flow, pressure ratio, and efficiency as a function of rotational speed. Usually two maps each are required for the compressor and turbine. The first map plots the pressure ratio versus dimensionless mass flow for a series of fixed (sometimes nondimensionalized) rotational speeds. The second map gives the normalized isentropic efficiency versus dimensionless mass flow

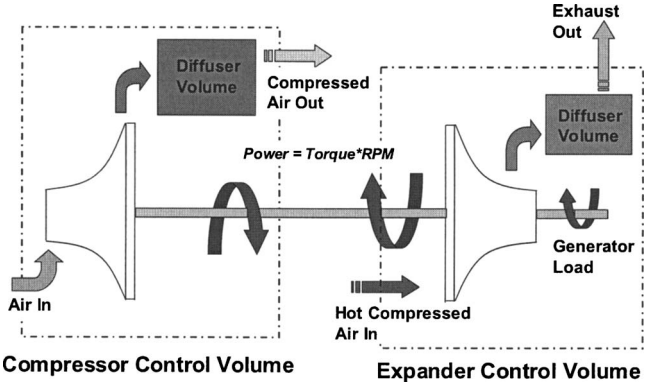

Fig. 4 Schematic approach to dynamic simulation of a gas turbine engine

for a series of fixed (sometimes nondimensionalized) rotational speeds. Typical nondimensionalization of the mass flow is as follows:

$$\frac{\dot{m}R\sqrt{\gamma RT_{01}}}{D^2P_{01}} \tag{23}$$

where $\dot{m}$ is the fluid mass flow, R is the gas constant, γ is the ratio of specific heats, T_{01} is the stagnation temperature at the inlet, D is a characteristic length, and P_{01} is the stagnation pressure at the inlet. Dimensionless rotor speed can be given by

$$\frac{ND}{\sqrt{\gamma RT_{01}}} \tag{24}$$

where N is the rotational speed.

Using the mapped compressor and turbine performance, the mass flow through such can be determined for any given speed, discharge pressure, and inlet condition. The solution strategy for both the turbine and compressor dynamics involves iterative determination of mass flow. For a given rotational speed and pressure ratio, a mass flow is guessed and iteratively converged upon until a pressure ratio matches the ratio of discharge pressure to inlet pressure. An iterative approach is necessary because the discharge pressure is determined by the swallowing capacity of components downstream of the compressor (or turbine). Once the mass flow is determined, a compressor (or turbine) efficiency can be determined from the efficiency map. Knowing the isentropic efficiency, the compressor (or turbine) exit temperature can be determined from the isentropic relations described in the following paragraphs.

The inlet temperature of the compressor is known, and once the compressor isentropic efficiency is extracted from the performance maps, the compressor stagnation exit temperature T_{02} can be calculated by using

$$T_{02} = T_{01}\left\{1 + \frac{1}{\eta_{\text{comp}}}\left[\left(\frac{P_{02}}{P_{01}}\right)^{\gamma-1/\gamma} - 1\right]\right\} \tag{25}$$

The specific heat C_P is calculated next as a function of temperature based on third-order curve fits for a gas mixture containing up to seven molecular species (CH_4, CO, CO_2, H_2, H_2O, N_2, O_2). Using C_P and the temperature of each state, the enthalpies can be calculated by Eq. (26) and used to calculate the compressor work using Eq. (27).

$$h_{01} - h_{02} = \int_{T_{02}}^{T_{01}} C_P(T)dT \tag{26}$$

$$P_C = \dot{m}_{\text{comp}}(h_{01} - h_{02}) \tag{27}$$

After the compressor exit state is determined, a dynamic expression that accounts for gas compressibility and mass storage in a separate compressor diffuser volume is solved as follows:

$$\frac{dP}{dt} = (\dot{m}_{\text{in}} - \dot{m}_{\text{out}})\frac{\gamma RT}{V} \tag{28}$$

Thus, for a given moment in time, all the parameters necessary to assess the dynamic compressor performance are calculated.

As for the gasifier turbine work or the turbine supplying work to the compressor, the turbine inlet temperature (T_{03}) is known. Using performance maps, the isentropic turbine efficiency can be extracted from the turbine efficiency map and used in Eq. (29) to calculate the turbine exit temperature

$$T_{04} = T_{03}\left\{1 + \eta_T\left[\left(\frac{P_{04}}{P_{03}}\right)^{\gamma-1/\gamma} - 1\right]\right\} \tag{29}$$

Once the temperatures are known then turbine mass storage can be assessed by solution of Eq. (28) for the turbine. Then the enthalpies at each state (Eq. (30)) are calculated in order to calculate the turbine power using Eq. (31)

$$h_{03} - h_{04} = \int_{T_{04}}^{T_{03}} C_P(T)dT \tag{30}$$

$$P_T = \dot{m}_{\text{comp}}(h_{03} - h_{04}) \tag{31}$$

The above calculations are performed at every time step in the gas turbine transient model. To capture the dynamics associated with the rotational inertia of the GT, the summation of torques is used to calculate the angular acceleration, which is integrated over time to calculate the shaft speed of the gasifier turbine. Equation (32) is solved with the known turbine and compressor powers, rotational inertia J, and rotational speed ω of the turbo machinery as follows:

$$\frac{d\omega}{dt} = \frac{1}{J\omega}(\mathrm{P}_{T_1} - \mathrm{P}_C) \tag{32}$$

For the second turbine (power turbine), the same equations are used to calculate the state (5 and 6) temperatures and enthalpies. As for the sum of the torques, the second shaft has the generator load instead of the compressor load as in Eq. (33).

$$\frac{d\omega}{dt} = \frac{1}{J\omega}(\mathrm{P}_{T_2} - \mathrm{P}_{\text{load}}) \tag{33}$$

The generator operates at 3600 rpm for 60 Hz AC electricity production; therefore, the load from the generator is dynamically adjusted to maintain the revolutions per minute of the power turbine at 3600 rpm. Due to alterations made to the nozzle of the gas turbine to accommodate the over-sizing of the gas turbine with the rest of the system the power turbine was operated at a lower number of revolutions per minute of 3000. This produced 50 Hz AC power from the generator.

Data-Model Comparison Approach

The MATLAB/SIMULINK modules described above were integrated into a system model that could simulate the 220 kW pressurized tubular SOFC/GT hybrid system of Fig. 1. The system configuration was identical to that presented in Fig. 2, with a fuel cell that was representative of the performance of an integrated SOFC/reformer module depicted in Fig. 3. Experimental start-up data are presented for model verification. A series of control moves must occur during start-up in order to heat up the fuel cell, control temperatures, and temperature ramp rates throughout the system, and maintain operation of the gas turbine. Two combustors were used to supply heat during start-up and SOFC stack warm-up. In the simulation results, the control moves that are identical to those recorded during the experiment were implemented in the simulation.

Results

The data, as stated earlier, that were acquired from the system and selected for simulation and comparison are system start-up data. During this period of operation, the SOFC/GT hybrid system was slowly ramped up in power to minimize the mechanical stresses from thermal shock. Figures 5–9 present the experimental and simulation data. Figure 5 presents the control moves made by the operator during start-up of the hybrid system. The controlled parameters were the SOFC load, recuperator and SOFC bypass, and the fuel flow to the system (SOFC load not shown in Fig. 5). The bypass valves were used to control the temperature of the SOFC stack. The recuperator bypass controlled the inlet temperature of the air entering the stack. The SOFC bypass was used to control the mass flow through the SOFC stack. The hybrid system utilized a dual-shaft turbine. As a result the total mass flow through the system could not be controlled independent of SOFC power. With a single-shaft gas turbine one can adjust turbomachinery speed (and thus compressor mass flow) by manipulation

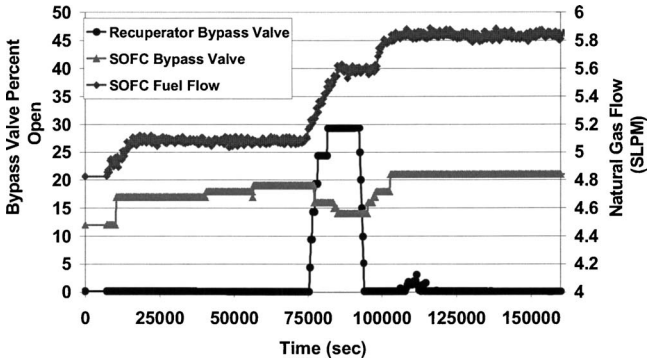

Fig. 5 Fuel flow and bypass valve positions used in the experiment and simulations

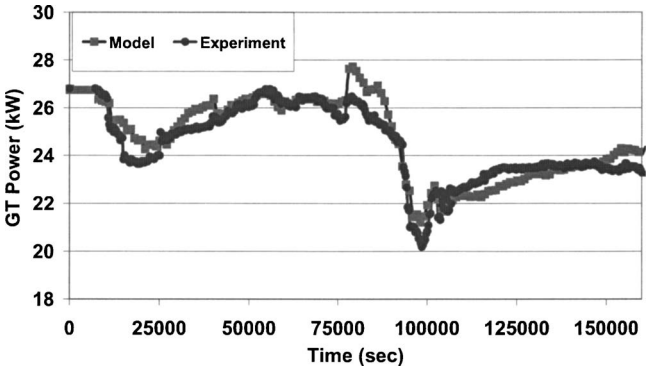

Fig. 7 Gas turbine power simulation and experimental data comparison

of generator load. The free-spinning turbine and compressor of the dual-shaft machine thus required an SOFC bypass flow to control speed (and mass flow).

In Fig. 6, the SOFC power is ramped up from 147 to 158 kW over a period of 100,000 s. The model simulation follows the SOFC power closely. The model input for the SOFC is the current demand and fuel flow rate. The cathode inlet temperature, operating fuel cell voltage, overall SOFC temperature, internal reformer temperature, combustor temperature, pressure, and other operating parameters are calculated and dependent on the solution of the integrated hybrid system dynamic performance as calculated using the simulation modules described herein. Sudden drops in SOFC power were observed in the experiment as the SOFC bypass valve was opened to allow more air to bypass the SOFC. At low load (time=10,000 s), the model does not capture this dynamic. However, a similar dynamic that occurs when the fuel cell is producing 157 kW (around t=90,000 s) is slightly captured by the model. It is believed these sudden drops in power are due to the changes in the airflows through and around the SOFC stack. The discrepancies of the experiment and model data during changes in the SOFC bypass valve position are due to uncertainties in the exact flow dynamics and flow amounts altered by the SOFC bypass valve.

Measurement data for the bypass valve position are not very accurate since the valve type used was a pneumatically actuated butterfly valve. Pressure, mass flow, and temperature deviations would lead to different mass flows being bypassed for the same valve position. Also the first degrees of movement of the valve dramatically change the amount of mass flow being bypassed. One could estimate the bypass mass flow using an enthalpy balance if accurate data for mass flow and temperatures around each bypass valves were known. Since this information was not available, bypass mass flow rates were estimated by valve position only with rates averaged over a 5 min time period.

The gas turbine performance, power output, system airflow rate, and SOFC pressure are each totally dependent on the SOFC performance (in model and experiment). The power output of the gas turbine (Turbine 2 of Fig. 2) is left to float depending on the SOFC stack exhaust conditions and the percentage of air that bypasses the SOFC. As more air bypasses the SOFC stack, the cooling of the SOFC stack decreases and the turbine inlet temperature (TIT) is reduced resulting in lower gas turbine power output. Figure 7 presents the experimental data and model results for the gas turbine power during the SOFC stack power ramp up. The model follows the power output of the gas turbine quite well with a few deviations during the SOFC stack ramp up. The model does not predict turbine power as accurately when the SOFC bypass valve is being adjusted. Some of the errors again are associated with the limited experimental data on actual bypassed mass flows.

The model well captures the change in the turbine inlet temperature (TIT) that corresponds to the SOFC ramp-up conditions as shown in Fig. 8. There is a slight error in the TIT that peaks at about 6 deg, but the overall trend is captured throughout the entire dynamic response to SOFC ramp-up perturbations.

Temperatures predicted by the dynamic model and observed in the experiment for several of the system states are presented in Fig. 9 for the starting and end-point conditions presented in previous figures. The temperatures throughout the system are fairly close, but there are some differences. There is a 5% difference in compressor mass flow, which could cause the model to predict lower temperatures, but instead the model predicts higher temperatures. The reason the model predicts higher temperatures is

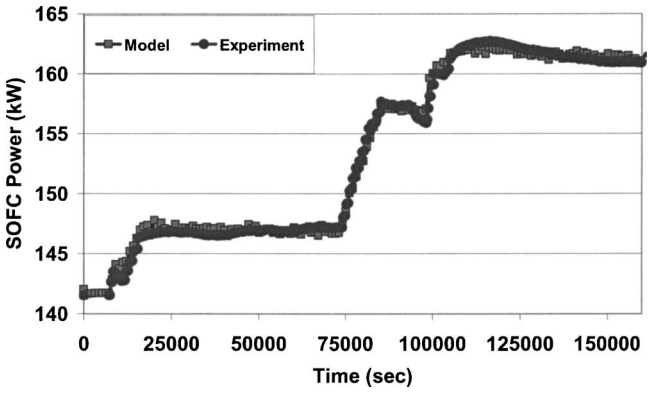

Fig. 6 SOFC power experimental and simulation comparison

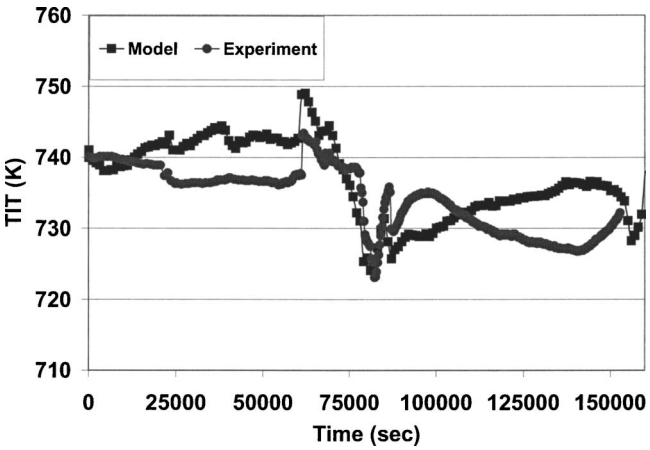

Fig. 8 Model and experiment turbine inlet temperature comparison

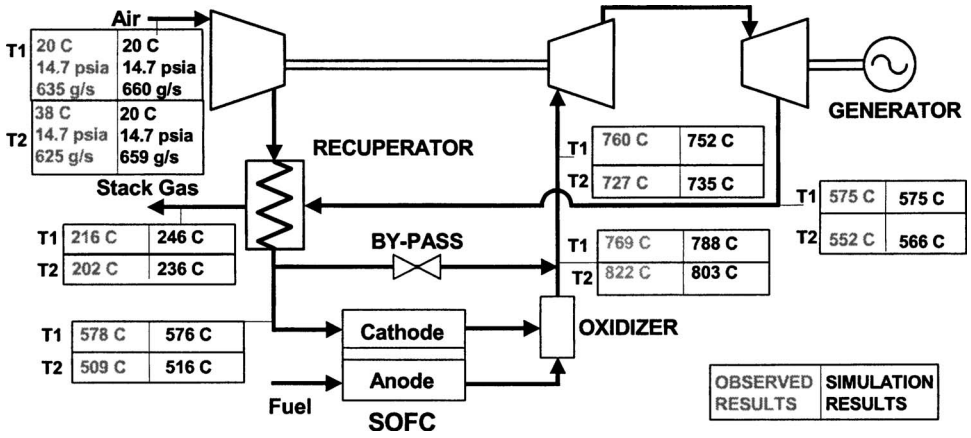

Fig. 9 Comparison of temperature states in hybrid system for initial and final conditions

due to inadequate accounting of the heat losses through out the system. The only heat losses currently considered in the system occur in combustors 1 and 2 (where there is significant heat loss). There are not any heat losses accounted for in the current SOFC and recuperator models, around which the largest temperature discrepancies are presented. Additional work is required in order to accurately quantify the heat losses associated with the SOFC stack and the recuperator. Nonetheless, the dynamic and steady-state performance predictions are impressive, given the system complexities.

Conclusions

A modular approach for dynamic simulation of the major system components of a hybrid FC/GT system is presented. The dynamic models were developed in a MATLAB/SIMULINK™ environment. Using the dynamic simulation modules, a detailed hybrid system model was constructed to simulate a 220 kW tubular SOFC/GT hybrid system. The dynamic model well captures the dynamic performance of the integrated experimental system for transient operating conditions observed during a system start-up. Some system dynamics are not well captured by the model, especially those associated with the bypass valve dynamics, which were not adequately understood at the time of model application. Overall, the dynamic model quite accurately captures the particular set of hybrid SOFC/GT performance data during a start-up transient. This comparison shows that the model, built from first principles, can reasonably predict the dynamic performance of a complex hybrid FC/GT system. Thus verified, the dynamic model can be used to provide operational insights and guidance for design and controls development. Comparisons of system simulation results to experimental data are rare in the literature, because of the dearth of available experimental results. Although the current paper does not fully validate the current system model, it provides confidence that users can apply the dynamic models in developing control algorithms and proper procedures for start-up and shutdown of these types of complex and integrated hybrid fuel cell systems. Future investigations will be performed to further validate the systems simulation tools and test the limits of component and system dynamic responses to load demands and other possible perturbations. Being able to test these scenarios with an accurate system model provides an insightful, economical, and safe means for system research and technology advancement.

Acknowledgment

Siemens Westinghouse, Department of Energy, California Energy Commission, National Fuel Cell Research Center.

Nomenclature

A_{cell} = fuel cell area (m^2)
C = concentration ($kmol/m^3$)
C_{mass} = specific heat (J/(kg K))
$C_p(T)$ = constant pressure specific heat (kJ/(kg K))
$C_{v,\text{molar}}$ = molar specific heat of gas (J/(kg K))
E = Nernst potential (V)
$\dot{E}_{\text{in}}$ = energy entering control volume (W)
E_o = ideal cell potential (V)
$\dot{E}_{\text{out}}$ = energy out of control volume (W)
F = Faraday's constant ($C/\text{mole}_{\text{electrons}}$)
f = friction coefficient (no unit)
h_{0i} = enthalpy at state i (kJ/kg)
i = cell current density (A/m^2)
i_o = exchange current density (A/m^2)
i_L = limiting current density (A/m^2)
J = polar moment of inertia ($kg\,m^2$)
$\dot{m}_{\text{comp}}$ = compressor mass flow rate (kg/s)
$\dot{N}$ = molar flow rate (kmol/s)
n = number of contributing electrons
P_C = compressor power (kW)
P_{cathode} = pressure of the cathode gas (atm)
P_{load} = generator load (kW)
P_{Ti} = power for turbine i (kW)
P_{0i} = stagnation pressure at state i (kPa)
Q_{gen} = energy generated in control volume (W)
R = reaction rate vector (kmol/s)
R_{eff} = internal cell resistance ($\text{ohm}\,m^2$)
R_u = ideal gas constant (J/(mol K))
T = temperature (K)
T_{0i} = stagnation temperature at state i (K)
V_{cell} = cell voltage (V)
V_{cv} = control volume (m^3)
$\mathbf{X}_i$ = species mole fraction vector (in or for control volume)
α = transfer coefficient
$\Delta H_{f,H_2O(g)}$ = heat of formation of water (J/mol)
ΔP = pressure drop (Pa)
γ = specific heat ratio

η_A = activation polarization (V)
η_{comp} = compressor efficiency
η_C = concentration polarization (V)
η_R = ohmic polarization (V)
υ = velocity of fluid (m/s)
ρ = density (kg/m^3)
ω = shaft angular speed (s^{-1})
χ_i = mole fraction of species i

References

[1] Hirschenhofer, J. H., Stauffer, D. B., and Engleman, R. R., 1994, *Fuel Cells—A Handbook (Revision 3)*, DOE/METC-94/1006.

[2] Massardo, A. F., and Lubelli, F., 2000, "Internal Reforming Solid Oxide Fuel Cell-Gas Turbine Combined Cycles (IRSOFC-GT): Part A—Cell Model and Cycle Thermodynamic Analysis," ASME J. Eng. Gas Turbines Power, **122**, pp. 27–35.

[3] Costamagna, P., Selimovic, A., Del Borghi, M., and Agnew, G., 2004, "Electrochemical Model of the Integrated Planer Solid Oxide Fuel Cell (IP-SOFC)," Chem. Eng. J., **102**, pp. 61–69.

[4] Costamagna, P., Magistri, L., and Massardo, A. F., 2000, "Design and Part-Load Performance of a Hybrid System Based on a Solid Oxide Fuel Cell Reactor and a Micro Gas Turbine," J. Power Sources, **96**, pp. 352–368.

[5] Bessette, N. F., 1994, "Modeling and Simulation for SOFC Power Systems," Georgia Institute of Technology, Atlanta, p. 209.

[6] Rao, A. D., and Samuelsen, G. S., 2002, "Analysis Strategies for Tubual Solid Oxide Fuel Cell Based Hybrid," ASME J. Eng. Gas Turbines Power, **124**, pp. 503–509.

[7] Yi, Y., Smith, T. P., Brouwer, J., and Rao, A. D., 2003, "Simulation of a 220 kW Hybrid SOFC Gas Turbine System and Data Comparison."

[8] Chan, S. H., Ho, H. K., and Tian, Y., 2002, "Modeling of Simple Hybrid Solid Oxide Fuel Cell and Gas Turbine Power Plant," J. Power Sources, **109**, pp. 111–120.

[9] Gemmen, R. S., Liese, E., Rivera, J. G., Jabbari, F., and Brouwer, J., 2000, "Development of Dynamic Modeling Tools for Solid Oxide and Molten Carbonate Hybrid Fuel Cell Gas Turbine Systems," ASME Turbo Expo, Munich, Germany, ASME Paper No. 2000-GT-0554.

[10] Liese, E. A., Gemmen, R. S., Jabbari, F., and Brouwer, J., 1999, "Technical Development Issues and Dynamic Modeling of Gas Turbine and Fuel Cell Hybrid Systems," ASME Turbo Expo, Indianapolis, ASME Paper No. 99-GT360.

[11] Liese, E. A., and Gemmen, R. S., 2002, "Dynamic Modeling Results of a 1 MW Molten Carbonate Fuel Cell/Gas Turbine Power System," 2002 ASME Turbo Expo, Amsterdam, ASME Paper No. GT-2002-30110.

[12] Lukas, M. D., Lee, K. Y., and Ghezel-Ayagh, H., 1999, "Development of a Stack Simulation Model for Control Study on Direct Reforming Molten Carbonate Fuel Cell Power Plant," IEEE Trans. Energy Convers., **14**(4), pp. 1651–1657 (PE-468-EC-0-01-1999).

[13] Lukas, M. D., Lee, K. Y., and Ghezel-Ayagh, H., 2000, *Operation and Control of Direct Reforming Fuel Cell Power Plant*, IEEE Power Engineering Society, New York.

[14] Ghezel-Ayagh, H., Daly, J. M., and Wang, Z.-H., 2003, "Advances in Direct Fuel Cell/Gas Turbine Power Plants," 2003 ASME Turbo Expo, Atlanta, ASME Paper No. GT2003-38941.

[15] Veyo, S. E., Lundberg, W. L., Vora, S. D., and Litzinger, K. P., 2003, "Tubular SOFC Hybrid Power System Status," *Proceedings of ASME Turbo Expo 2003*, ASME, New York, ASME Paper No. GT2003-38943.

[16] Roberts, R. A., Brouwer, J., Gemmen, R., and Liese, E., 2003, "Inter-Laboratory Dynamic Modeling of a Carbonate Fuel Cell for Hybrid Application," 2003 ASME Turbo Expo, Atlanta, ASME Paper No. GT2003-38774.

[17] Roberts, R. A., Brouwer, J., Gemmen, R., and Liese, E., 2004, "Dynamic Simulation of Carbonate Fuel Cell-Gas Turbine Hybrid Systems," ASME Turbo Expo, Vienna, ASME Paper No. GT2004-53653.

[18] Xu, J., and Froment, G. F., 1989, "Methane Steam Reforming, Methanation and Water-Gas Shift: I. Intrinsic Kinetics," AIChE J., **35**(1), pp. 88–96.

[19] Weber, A., Bastain, S., Muller, A. C., Herbstriitt, D., and Ivers-Tiffee, E., 2002, "Oxidation of H_2, CO and Methane in SOFCs With Ni/YSZ-Cermet Anodes," Solid State Ionics, **152–153**, pp. 543–550.